THE JOURNAL OF NAVIGATION (2018), **71**, 878–898. © The Royal Institute of Navigation 2018
doi:10.1017/S0373463318000024

Course keeping Control Based on Integrated Nonlinear Feedback for a USV with Pod-like Propulsion

Yunsheng Fan[1], Dongdong Mu[1], Xianku Zhang[2], Guofeng Wang[1] and Chen Guo[1]

[1] *(Information Science and Technology College, Dalian Maritime University, Dalian, China)*
[2] *(Navigation College, Dalian Maritime University, Dalian, China)*
(E-mail: yunsheng@dlmu.edu.cn)

In this paper, a response model of an Unmanned Surface Vehicle (USV) with a pod-like propulsion device is established. To improve the robustness of motion control in heavy sea states, an integrated nonlinear feedback course-keeping controller is proposed. First, to establish a response model of a USV with pod-like propulsion, model parameters are obtained by the method of system identification, then an integrated nonlinear feedback control strategy is proposed. The essence of this method is to make the original error signal pass through a nonlinear function, and then the output of this function is used to replace the original error signal. Simulation results show that under ordinary sea states, nonlinear feedback can save up to 34.5% of energy used compared with standard feedback methods; under heavy sea states, this can rise to 40.8%. A set of field experiments were carried out with a USV with pod-like propulsion. Results show that under heavy sea states, the test USV can maintain the target course well, which proves the correctness of the model and the robustness of the proposed method.

KEYWORDS

1. USV. 2. Pod-like propulsion. 3. Model Parameters Identification. 4. Course Keeping Control. 5. Integrated Nonlinear Feedback.

Submitted: 8 April 2017. Accepted: 29 December 2017. First published online: 13 February 2018.

1. INTRODUCTION. Unmanned Surface Vehicles (USVs) are developing rapidly and becoming smaller, faster and more energy efficient. Their greatest advantage is that they are able to accomplish predetermined tasks independently (Fan et al., 2015). They can be used in military or civilian fields, such as enemy warship tracking, marine monitoring, ocean surveillance, ocean exploration and signal transfer (Sarda et al., 2015). In order to better accomplish tasks in the complex ocean environment, ever higher performance is required of USVs' propulsion systems. Pod-like propellers, which are essentially vector propulsion

https://doi.org/10.1017/S0373463318000024 Published online by Cambridge University Press

devices that can direct thrust over a wide range of directions, are a new type of propulsion device, which can save space and improve propulsion efficiency. With pod-like propellers, vessels can achieve rotation, reverse and horizontal movements without the use of separate rudders, propellers or fixed thrusters (Skjetne et al., 2004). Pod-like propellers represent one of the most promising new technologies in the field of ship propulsion (Sakuma and Naruse, 2016). For a USV, pod-like propellers not only meet the basic requirements for motion control, but can also improve performance and manoeuvrability. In principle, pod-like propulsion is different from the traditional fixed propeller-rudder combination, so the first step of this paper is to establish the response model of a USV with pod-like propulsion, and then the system identification method is employed to obtain the model parameters.

The design of a course-keeping controller is an important research topic of ship motion control, because it is not only related to the economy and security of the vessel's operation, but also the foundation of a USV's autonomous navigation. Fang and Luo (2007) proposed a Sliding Mode Control (SMC) course-keeping controller, but the SMC high frequency chattering phenomenon is difficult to solve. In order to tackle this, Gao and Chen (2010) used fuzzy control to optimise the gain of a sinusoidal function to reduce the chattering phenomenon, and simulation results show that its control effect is better than the traditional SMC control. A fast non-singular terminal sliding mode course controller, consisting of a linear sliding mode and a non-singular terminal sliding mode, was proposed by Mu et al. (2017). At the same time, the universal approximation capability of Radial Basis Function (RBF) neural networks was used to solve chattering problem for control inputs. Li et al. (2013) combined SMC and Active Disturbance Rejection Control (ADRC) to design a ship course controller, and the sideslip angle caused by wave current was solved by means of coordinate transformation. In Yuan and Wu (2010), backstepping and terminal sliding mode were combined to design the course controller, and the fuzzy approximation method was used to solve the model uncertainty. Du et al. (2006) adopted a backstepping adaptive algorithm to design a course-keeping controller, but the inherent backstepping "computation explosion" problem has brought great difficulty to the design of an appropriate controller. In view of this problem, Wang and Huang (2005) used a dynamic surface technique to solve the problem of multiple derivatives of virtual control laws effectively.

In practical engineering, there is a very important problem that needs to be taken into consideration, that is, the input saturation of the actuator. Li et al. (2012) designed a ship course-keeping controller based on backstepping, and neural network approximation was used to solve the problem of model uncertainty. Although researchers (Li et al., 2017; Li and Tong, 2016; Tong et al., 2014; Peng et al., 2016) have extensively studied controller design, these so-called advanced algorithms are difficult to apply to practical engineering. In order to simplify the design of a controller, Zhang and Zhang (2016) proposed a nonlinear feedback strategy. At the same time, Zhang et al. (2017) have completed further research on a nonlinear feedback strategy. Combining this with backstepping techniques, a nonlinear feedback course controller was proposed. However, after an actual ship experiment, we found that the nonlinear feedback strategy of Zhang et al. (2017) may be better suited to large merchant ships. Proportional-Derivative (PD) control is the scheme most widely used in practical engineering, but in the presence of external interference, the frequency of the rudder's movement is very high. This behaviour not only reduces the life of the drive motor, but also uses more energy.

https://doi.org/10.1017/S0373463318000024 Published online by Cambridge University Press

In this paper, motivated by the above-mentioned observations, a practical integrated nonlinear feedback course-keeping course control strategy is developed for a USV with pod-like propulsion. Because the nonlinear feedback strategy is optimised on the basis of PD control, it is simple in structure and easy to implement. The main contributions of this paper can be summarised as follows:

(1) In contrast to ordinary merchant ships, a USV is small in size, fast in speed and weak in resisting external disturbances, so when we design a USV course controller, we should first consider its ability to resist external interference. Therefore, a novel nonlinear feedback course controller with strong robustness is proposed and applied to a USV with pod-like propulsion.
(2) A course-keeping controller combined with nonlinear feedback and classical PD control has the advantages of simple structure and easy implementation. In simulation, it is proved that under ordinary sea conditions, nonlinear feedback can save 34.5% energy compared to a standard feedback system; under heavy sea conditions, this can rise to a 40.8% energy saving.
(3) The greatest advantage of this paper lies in integrating theory with practice. Under heavy sea conditions, the nonlinear feedback course controller is applied to real vessel experiments, and good control results are obtained. The correctness and effectiveness of the proposed method are proved by theoretical simulation and practical application.

The rest of the paper is organised as follows. Section 2 introduces the modelling problem of a USV with pod-like propulsion. In Section 3, the parameters of the response model are identified and verified. Section 4 introduces our nonlinear feedback theory. In Section 5, numerical simulations are carried out to show the correctness and robustness of this theory. In Section 6, the nonlinear feedback course-keeping controller is tested under heavy sea states in a real vessel experiment. Finally, conclusions are made and future research directions are introduced in Section 7.

2. USV MODELLING.

At present, there are two main types of ship manoeuvring motion modelling: the integral model proposed by Abkowitz (1964) and the separation model proposed by the Ship Manoeuvring Mathematical Model Group (MMG). The separation model is also called the MMG model (Jia and Yang, 1999). The main idea of the MMG model is to consider the force of the hull and the thrust of the actuator separately, and each variable has a clear physical meaning. Based on this, the MMG model is employed to study the mathematical model of the *Lanxin* USV.

2.1. *Lanxin USV and its pod-like propeller.*

The *Lanxin* USV is a 7.02 m long intelligent equipment platform owned by Dalian Maritime University, which has the functions of water sampling, marine monitoring, maritime rescue, etc. (Fan et al., 2015). The *Lanxin* USV is shown in Figure 1.

It can be seen from Figure 2 that when the propeller changes its propulsion angle, the vectored thrust produced by the propeller can be decomposed into two directions: forward thrust component which propels the vessel forward and a lateral thrust component which achieves steering.

2.2. *Planar motion model.*

Conventionally, the Earth-fixed frame and the body-fixed frame are adopted to study the USV model. As shown in Figure 3, $O - X_0Y_0Z_0$ is the

https://doi.org/10.1017/S0373463318000024 Published online by Cambridge University Press



Figure 1. *Lanxin* USV.



Figure 2. The pod-like propeller of *Lanxin* USV.

https://doi.org/10.1017/S0373463318000024 Published online by Cambridge University Press

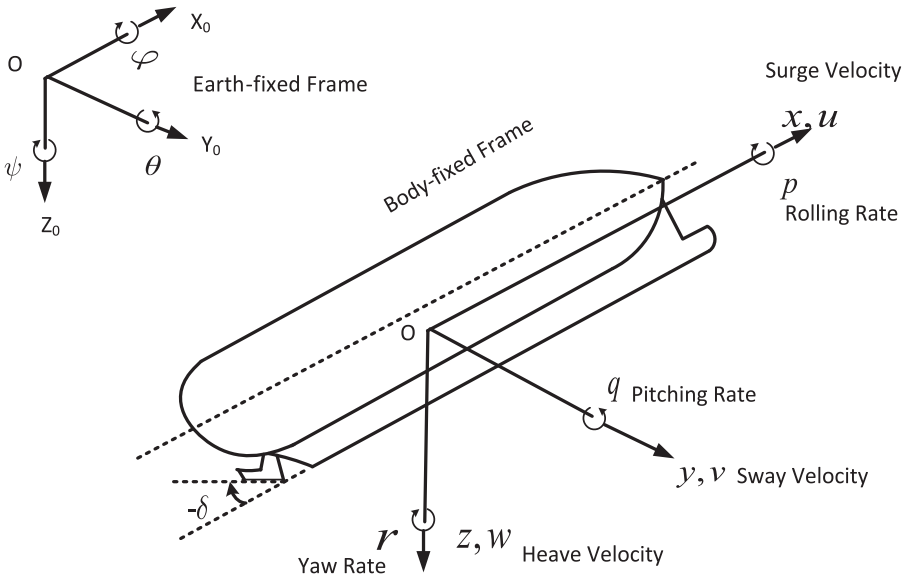


Figure 3. The Earth-fixed frame and the body-fixed frame.

inertial coordinate system and $o-xyz$ is the attached body coordinate system. The USV has six Degrees Of Freedom (DOFs) including surge velocity u, sway velocity v, heave velocity w, yaw rate r, roll rate p and pitch rate q. ψ is course angle and δ is propulsion angle.

In planar motion modelling, heave velocity, roll rate and heave velocity are not taken into account. Here, we assume that the USV is symmetrical, and the origin of the attached coordinate system and the barycentre of the USV are coincident. The planar motion model of three DOFs can be represented as

$$\begin{cases} (m+m_x)\dot{u} - (m+m_y)vr = X \\ (m+m_y)\dot{v} + (m+m_x)ur = Y \\ (I_{zz}+J_{zz})\dot{r} = N \end{cases} \tag{1}$$

where m is the mass of the USV, m_x is the additional mass in the x-axis direction, m_y is the additional mass in the y-axis direction, I_{zz} is the moment of inertia of the o_z axis, J_{zz} is the additional moment of inertia in the direction of the z-axis and X, Y and N are the hydrodynamic forces and moments acting on the hull. According to Jia and Yang (1999), X, Y and N can be divided as in Equation (2) and the USV's hydrodynamic forces are shown in Equation (3).

$$\begin{cases} X = X_H + X_p \\ Y = Y_H + Y_p \\ N = N_H + N_p \end{cases} \tag{2}$$

https://doi.org/10.1017/S0373463318000024 Published online by Cambridge University Press

where the subscript H is the hydrodynamic force acting on the bare hull and P is the propulsor force.

$$\begin{cases} X_H = X(u) + X_{Hvv}v^2 + X_{Hvr}vr + H_{Hrr}r^2 \\ Y_H = Y_{Hv}v + Y_{Hr}r + Y_{NL} \\ N_H = N_{Hv}v + N_{Hr}r + N_{NL} \end{cases} \tag{3}$$

where Y_{NL} and N_{NL} are nonlinear fluid dynamic factors, and if they are considered as a high order small quantity, they can be ignored. H_{Hvv}, H_{Hvr} and H_{Hrr} are the viscous fluid dynamic coefficients in the direction of X; Y_{Hv} and Y_{Hr} are the viscous fluid dynamic coefficients in the direction of Y; N_{Hv} and N_{Hr} are the viscous fluid dynamic coefficients in the direction of N. In general, their values can be obtained by means of theoretical calculation or by constrained ship model experiments (Jia and Yang, 1999).

According to Sonnenburg and Woolsey (2013), when the propulsion angle δ is small, the thrust vectors in different directions are

$$\begin{cases} X_P = (cV\delta_n + d|\delta_n|\delta_n) \\ Y_P = (cV\delta_n + d|\delta_n|\delta_n)\delta \\ N_P = x_p(cV\delta_n + d|\delta_n|\delta_n)\delta \end{cases} \tag{4}$$

where V is the speed of the USV, δ_n is the rotation speed of the propeller, c and d are coefficients that are greater than zero and x_p is the length from the centre of rotation to the fulcrum of the propeller.

2.3. *Derivation and simplification.* Assume the longitudinal initial velocity of the USV is $u = u_0$, $v = 0$, $r = 0$ and $\delta = 0$. When the USV is disturbed by interference, $u = u_0 + \Delta u$, $\Delta v = v$, $\Delta r = r$ and $\Delta\delta = \delta$. Then Equation (1) can be simplified as

$$\begin{cases} (m + m_x)\Delta\dot{u} = X \\ (m + m_y)\dot{v} + (m + m_x)u_0 r = Y \\ (I_{zz} + J_{zz})\dot{r} = N \end{cases} \tag{5}$$

Keeping first order small quantities Δu, v, r, δ and ignoring higher order small quantities,

$$\begin{cases} X_H = -\frac{1}{2}\rho S C_t(u_0 + \Delta u)^2 \\ Y_H = Y_{Hv}v + Y_{Hr}r \\ N_H = N_{Hv} + N_{Hr}r \end{cases} \tag{6}$$

where X_H is the direct resistance of the USV, S is the wet area of the USV, ρ is water density and C_t is the total drag coefficient. Its specific expression is Equation (7).

$$X_H = -\frac{1}{2}\rho S[C_{t0} + \left(\frac{\partial C_t}{\partial \Delta u}\right)_{u0}\Delta u](u_0 + \Delta u)^2 \tag{7}$$

When the initial speed is u_0, the total resistance coefficient can be expressed as C_{t0}. Meanwhile, we define $X_0 = -\frac{1}{2}\rho S C_{t0}u_0^2$ and $X_{Hu} = -\frac{1}{2}\rho S[2C_{t0}u_0 + (\frac{\partial C_t}{\partial \Delta u})_{u0}u_0^2]$, then the Δu of

https://doi.org/10.1017/S0373463318000024 Published online by Cambridge University Press

Equation (7) is linearized as

$$X_H = X_0 + X_{Hu}\Delta u \tag{8}$$

where X_0 is the straight line resistance of the unmanned vehicle in the initial state. Equation (6) can be simplified as

$$\begin{cases} X_H = X_0 + X_{Hu}\Delta u \\ Y_H = Y_{Hv}v + Y_{Hr}r \\ N_H = N_{Hv} + N_{Hr}r \end{cases} \tag{9}$$

Substitute Equations (4) and (9) into Equation (2), and under the initial condition, $X_0 + X_P = 0$. We can get Equation (10):

$$\begin{cases} X = X_u\Delta u \\ Y = Y_{Hv}v + Y_{\mathrm{Hr}}r + X_p\delta \\ N = N_{Hv}\mathrm{v} + N_{Hr}r + x_{\delta s}X_p\delta \end{cases} \tag{10}$$

Substituting Equation (10) into Equation (5) results in

$$\begin{cases} (m + m_x)\Delta\dot{u} = X_u\Delta u \\ (m + m_y)\dot{v} + (m + m_x)u_0 r = Y_{Hv}v + Y_{\mathrm{Hr}}r + X_p\delta \\ (I_{zz} + J_{zz})\dot{r} = N_{Hv}\mathrm{v} + N_{Hr}r + x_{\delta s}X_p\delta \end{cases} \tag{11}$$

For ship course control, we pay more attention to the relationship between the course and the propulsion angle, so we only analyse the third formula of Equation (11). We define $Y_{\mathrm{Hv}} = Y_v$, $Y_{Hr} = Y_r$, $X_{\mathrm{p}} = Y_\delta$, $N_{Hv} = N_v$, $N_{Hr} = N_r$, $x_{\delta s}X_p = N_\delta$, then the third formula of Equation (11) can be simplified as

$$(I_{zz} + J_{zz})\dot{r} = N_v v + N_r r + N_\delta\delta \tag{12}$$

In order to simplify the problem, assuming that the initial state is uniform motion, and all the motion variables have zero initial value, then $\Delta u(0) = 0$, $v(0) = 0$, $r(0) = 0$, $\dot{v}(0) = 0$, $\dot{r}(0) = 0$, $\delta(0) = 0$ and $\dot{\delta}(0) = 0$.

After Laplace transformation, Equation (12) is converted to Equation (13).

$$(I_{zz} + J_{zz})sr(s) = N_v v(s) + N_r r(s) + N_\delta\delta(s) \tag{13}$$

According to Jia and Yang (1999), Equation (13) can be simplified as Equation (14).

$$T_1T_2\dot{r} + (T_1 + T_2)\dot{r} + r + \alpha r^3 = K\delta + KT_3\dot{\delta} \tag{14}$$

where α is a newly introduced constant and T_1, T_2, T_3 and K are the corresponding parameters. Equation (14) is simplified to a first-order system (15).

$$T\dot{r} + r + \alpha r^3 = K\delta \tag{15}$$

From this we can see that the response model of a USV with pod-like propulsion conforms to the Norrbin model structure (Norrbin, 1971) just like as an ordinary propeller-rudder propulsion ship.

https://doi.org/10.1017/S0373463318000024 Published online by Cambridge University Press

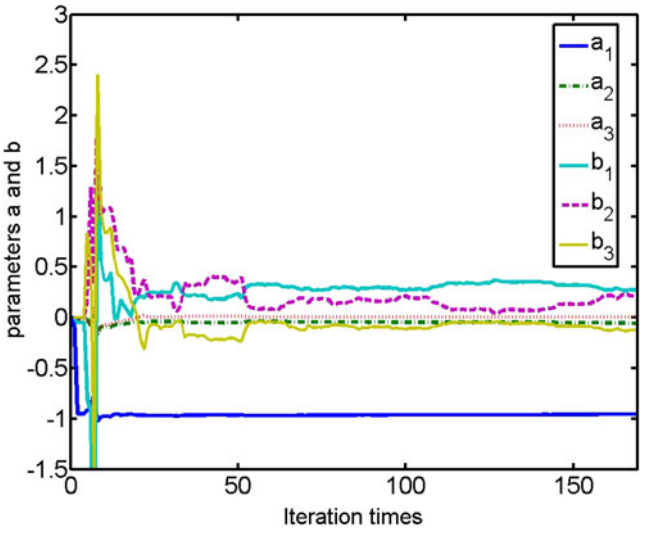


Figure 4. Identification curves.

2.4. *Servo system model.* In this paper, a two order, less damped model is used to replace the traditional first-order inertial model to describe the servo system model:

$$\ddot{\delta} + 2\zeta\omega_n\delta + \omega_n^2\delta = \Xi\omega_n^2\delta_r \tag{16}$$

where ω_n is the natural frequency, ζ is the damping ratio, Ξ is the coefficient of proportion and δ_r is the target propulsion angle.

3. MODEL IDENTIFICATION AND VERIFICATION.

3.1. *Parameter identification of response model.* Collecting data through field experiments is the basis of system identification. Field experiments include 5°, 8°, 12°, 15°, 17°, 18°, 20° turning tests and 15°/15° zig-zag tests. It is of note that field experiments need to be carried out in a relatively stable sea surface. The essence of the Norribin model is a linear Nomoto model with a nonlinear term α, so K and T can be obtained by identifying the Nomoto model. Equation (17) is the Nomoto model (Nomoto et al., 2009).

$$T\dot{r} + r = K\delta \tag{17}$$

Based on 15°/15° zig-zag test data, the Nomoto model is identified by recursive least squares. The identification curves are displayed in Figure 4.

$a_1 \sim a_3$ and $b_1 \sim b_3$ are the coefficients of the discrete transfer function. The transfer function is

$$\frac{0.2743z^2 + 0.2122z - 0.118}{z^3 - 0.9537z^2 - 0.5476z + 0.007182} \tag{18}$$

Equation (18) is converted to a continuous transfer function Equation (19).

$$\frac{1.65s^3 - 10.63s^2 + 88.19s + 225.9}{s^4 + 14.26s^3 + 106.8s^2 + 322s - 0.7904} \tag{19}$$

https://doi.org/10.1017/S0373463318000024 Published online by Cambridge University Press

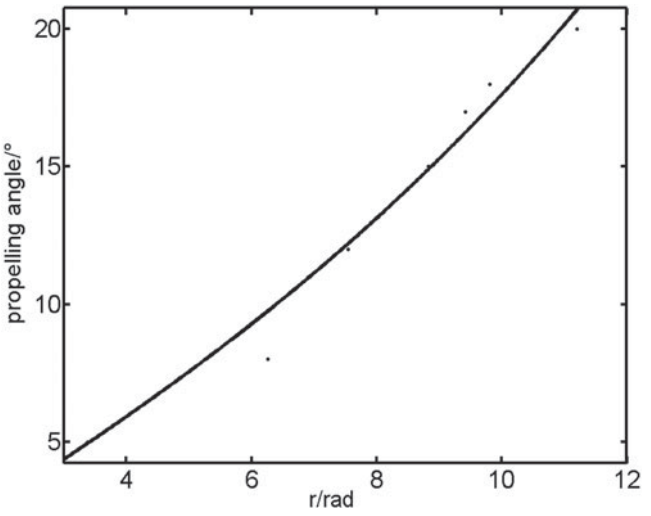


Figure 5. Fitting curve.

Due to the higher order and lower order coefficients differing greatly, Equation (19) can be simplified as Equation (20).

$$\frac{225.9}{106.8s^2 + 332s} \tag{20}$$

Equation (17) is changed to a transfer function and then compared with Equation (20), we can obtain $K = 0.707$ and $T = 0.332$. α is fitted by using turning test data, and during the turning test, $\dot{r}$, $\ddot{r}$ and $\ddot{\delta}$ are equal to zero, so Equation (15) can be simplified as Equation (21).

$$\alpha r^3 + r = K\delta \tag{21}$$

It can be seen from Equation (21) that when K is known, we can use multiple groups of δ and r to fit the α. As described in the above, a series of turning tests are designed to obtain multiple groups of δ and r. The fitting curve is shown in Figure 5, and the final result is $\alpha = 0.001$.

3.2. *Parameter identification of servo system model.* 15°/15° zig-zag test data are used to identify the servo response model of the system, and the convergence curves are shown in Figure 6.

a_1, a_2 and b_1, b_2 are the coefficients of the discrete transfer function. The transfer function is shown in Equation (22).

$$\frac{-0.2724z + 0.8464}{z^2 + 1.553z + 0.9169} \tag{22}$$

Equation (22) is transformed into a continuous transfer function.

$$\frac{\delta}{\delta_r} = \frac{0.923 \times 0.985^2}{s^2 + 2 \times 0.811 \times 0.985 + 0.985^2} \tag{23}$$

The average value of natural frequency $\omega_n = 0.958$, the average value of damping ratio $\zeta = 0.811$, the average value of the amplification factor $\Xi = 0.923$.

https://doi.org/10.1017/S0373463318000024 Published online by Cambridge University Press

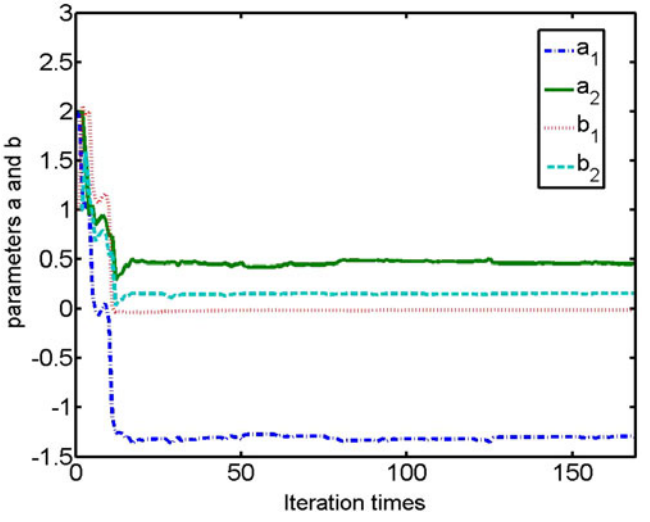


Figure 6. Servo system identification.

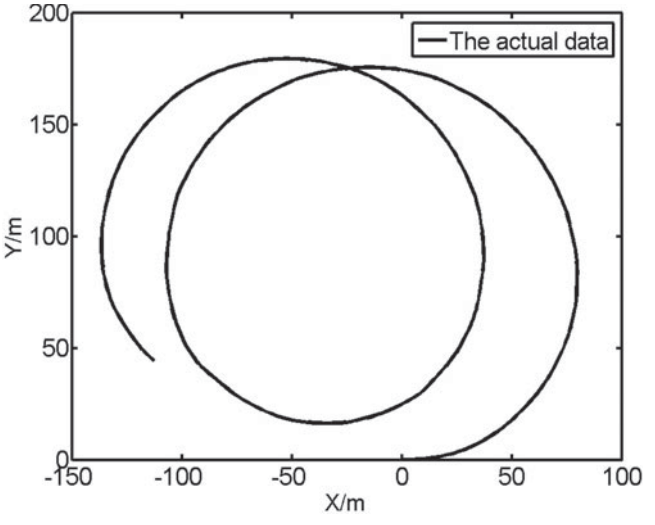


Figure 7. Actual turning test curve.

3.3. *Model validation.*

3.3.1. *Turning test verification.* To verify the correctness of the identification results, a simulated 5° turning test is carried out and compared with the actual data. The actual turning test curve is shown in Figure 7 and the simulated turning test curve is shown in Figure 8.

As can be seen from Figures 7 and 8, the actual radius of gyration is 85.2 m and the simulation gives 86.1m. Due to external disturbances, trajectory drift occurs in the actual turning test. The absolute error between them is 1%.

3.3.2. *Z type test verification.* A simulated 15°/15° zig-zag test was carried out and compared with the actual data. Comparison results are shown in Figures 9 and 10.

https://doi.org/10.1017/S0373463318000024 Published online by Cambridge University Press

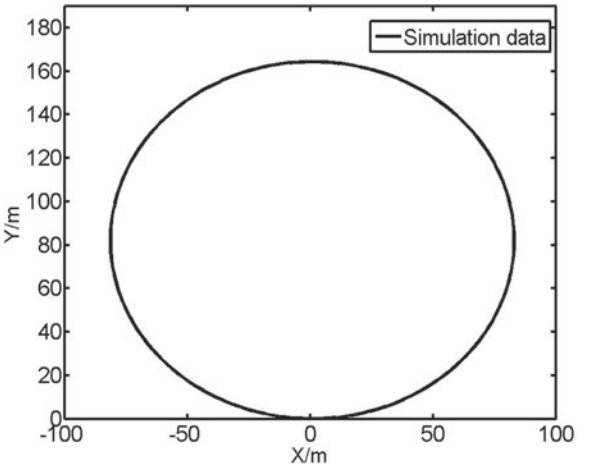


Figure 8. Simulation turning test curve.

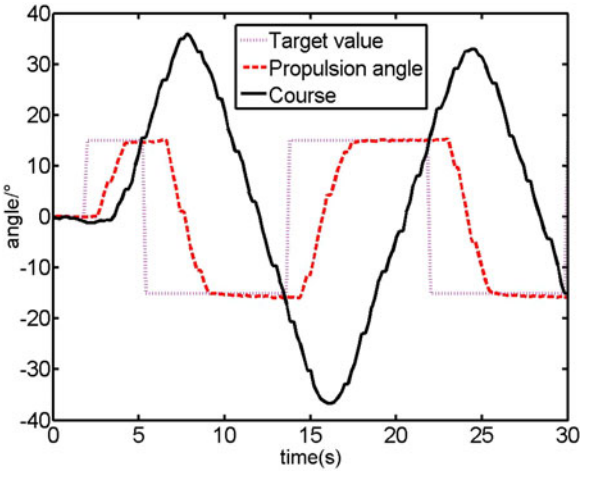


Figure 9. Actual zig-zag test curve.

It can be seen from Figures 9 and 10 that the actual propulsion angle period is about 12 seconds and the simulated one is about 11.5 seconds. From this, it can be concluded that the two order, less damped model is in line with the actual servo system, and the identification results are credible.

4. NONLINEAR FEEDBACK. In this chapter, a nonlinear feedback strategy is introduced to optimise the control effect. A nonlinear feedback control system driven by the square of the error and inverse sine function of the error is shown in Figure 11.

x_c is the input, y_c is the output, $x_c - y_c$ is the error, ω is system frequency, a is a coefficient less than 1, G represents the model of the controlled plant and M is the controller. The difference between nonlinear feedback and standard feedback is that the error $x_c - y_c$ is

https://doi.org/10.1017/S0373463318000024 Published online by Cambridge University Press

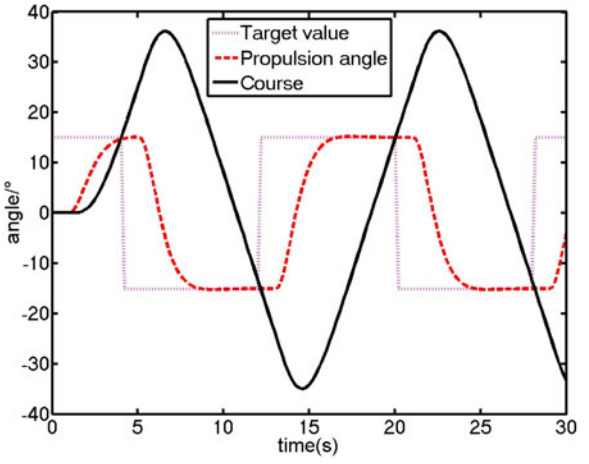


Figure 10. Simulated zig-zag test curve.

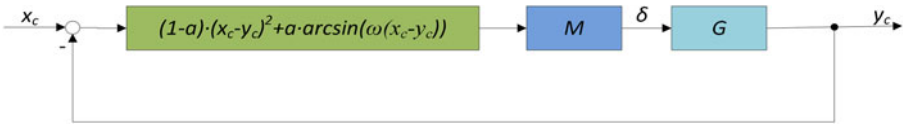


Figure 11. Nonlinear feedback structure.

replaced by $(1-a)\times(x_c-y_c)^2+a\times\arcsin(\omega(x_c-y_c))$. For a USV course-keeping system, G is the Nomoto model. M is designed using a first order closed-loop gain shaping algorithm (Zhang and Zhang, 2016; Zhang and Jia, 2002), and the bandwidth of the closed-loop system is set to $\frac{1}{T_1}$. When the closing slope is -20dB/dec, a closed loop gain shaping controller for a standard feedback system is designed, and the singular value curve of the closed-loop spectrum is approximated as the frequency spectrum of the first order inertia system with the largest singular value of one. Then

$$\frac{1}{T_1 s+1}=\frac{GM}{1+GM} \tag{24}$$

Next, the course-keeping controller can be obtained.

$$M=\frac{1}{GT_1 s} \tag{25}$$

In the USV course-keeping system, propulsion angle δ is the input and course ψ is the output. The Nomoto model Equation (17) in the time domain is converted to the frequency domain.

$$G(s)=\frac{K}{s(Ts+1)} \tag{26}$$

Substituting Equation (26) into Equation (25), according to the closed-loop gain shaping algorithm, a linear PD controller is obtained (M is in essence a PD controller).

$$M=\frac{1}{KT_1}+\frac{T}{KT_1}s \tag{27}$$

https://doi.org/10.1017/S0373463318000024 Published online by Cambridge University Press

When $|x_c - y_c| \leq \frac{\pi}{4}$, we discuss the advantages of nonlinear feedback in three cases.

Case 1: Define $(x_c - y_c)^2 = A$. As $|x_c - y_c| \leq \frac{\pi}{4}$ and $(1 - a) < 1$, then $(1 - a)A$ is much smaller than $\frac{\pi}{4}$. That is to say, this nonlinear term reduces the error signal to a certain extent. As for the PD controller, the decrease of the error signal means the weakening of control, which can make the control process more stable. In course-keeping control for a real ship, "steady" is more important than "fast".

Case 2: We define $\frac{\pi}{4}$ as a small error, so $a \arcsin(\omega(x_c - y_c))$ can be approximately equal to $a\omega(x_c - y_c)$.

According to the final value theorem, the steady-state output of the system in Figure 11 can be expressed as

$$y_c(\infty) = \lim_{s\to 0} s\frac{GMa\omega}{1 + GMa\omega}\frac{x_c}{s} = \lim_{s\to 0}\frac{(\frac{1}{T_1 s} + \frac{K}{s(Ts+1)})a\omega}{1 + (\frac{1}{T_1 s} + \frac{K}{s(Ts+1)})a\omega}x_c$$
$$= \lim_{s\to 0}\frac{(Ts + KT_1 + 1)a\omega}{TT_1 s^2 + T_1 s + (Ts + KT_1 + 1)a\omega}x_c = x_c \tag{28}$$

Then the output steady-state error is

$$x_c - y_c(\infty) = x_c - x_c = 0 \tag{29}$$

It can be proved that a nonlinear feedback driven by an inverse sine function does not affect the steady state of the system.

Remark 1. In field experiments, especially in the presence of strong environmental interference, $\frac{\pi}{4}$ is not considered a large value. Based on this situation, Case 2 is reasonable.

Case 3: The transfer function of system input x_c (target course) and the system output y_c (real-time course) is

$$\frac{y_c}{x_c} = \frac{GM\omega}{1 + GM\omega} \tag{30}$$

Sea waves are high frequency interference, with a spectrum range of $0.3 \sim 1.25$ rad/s (Zhang, 2011). When designing the inverse sine function, its system frequency ω should avoid the spectrum of sea waves. In this paper, $\omega = \frac{1}{45} \approx 0.022$. According to the closed loop gain shaping theory, the open-loop frequency characteristics of the system GM meet the requirements of low frequency high gain and high frequency low gain.

5. CASE STUDIES.

In this section, some numerical simulations are carried out to demonstrate the effectiveness of the proposed control scheme. The simulation diagram is shown in Figure 12.

Taking the *Lanxin* USV as an example, the corresponding model parameters are identified in Section 3. Meanwhile, the nonlinear feedback PD controller proposed is compared with the sine function nonlinear feedback PD controller (Zhang and Zhang, 2016) and standard feedback PD controller to prove the correctness of the point of view in this paper. The PD controller is shown in Equation (31).

$$\delta = K_p e + K_d \dot{e} \tag{31}$$

where K_p and K_d are positive design parameters and e can represent the error of standard or nonlinear feedback, respectively. The parameters of the nonlinear feedback PD controller

https://doi.org/10.1017/S0373463318000024 Published online by Cambridge University Press

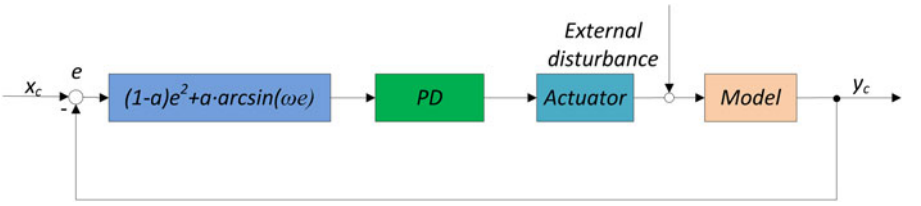


Figure 12. Simulation diagram.

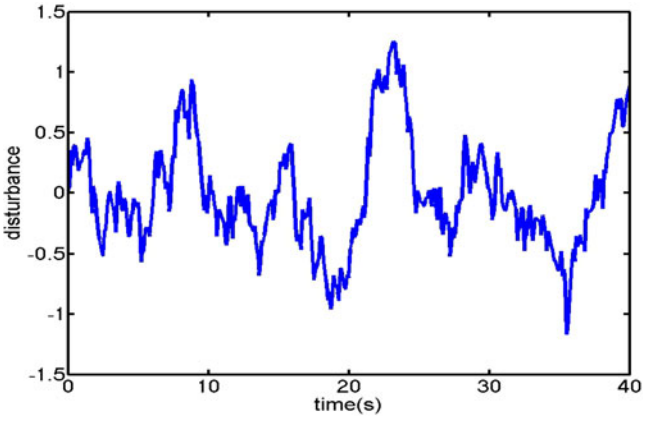


Figure 13. External disturbance curve.

proposed are set to $K_p = 0.9$, $K_d = 0.2$, $a = 0.28$ and $\omega = \frac{1}{45}$. The parameters of the sine function nonlinear feedback PD controller are set to $K_p = 0.9$, $K_d = 0.2$ and $\omega = \frac{1}{45}$. The parameters of the standard feedback PD controller are set to $K_p = 0.9$, $K_d = 0.2$. To show the results of comparison more clearly, an Integration of Time and Absolute Error (ITAE) performance evaluation index is employed to describe the propulsion angle. The ITAE can be represented as

$$\text{ITAE} = \int_0^t t|e(t)|dt \tag{32}$$

The original intention of the nonlinear feedback is to reduce the influence of external disturbance on the control system. A transfer function $L(s)$ is driven by a white noise with a zero mean to express external disturbance when the sea wind is Force 5 (Beaufort scale) (Yang et al., 2001).

$$L(s) = \frac{0.42s}{s^2 + 0.36s + 0.37} \tag{33}$$

The external disturbance curve is shown in Figure 13.

Comparison results are shown in Figures 14 and 15, and the ITAE index of the propulsion angle is shown in Table 1.

Remark 2. The benchmark of the ITAE index of propulsion angle is zero.

From Figure 14, it is clear that all systems have almost the same control effect when all the control parameters are the same, but the convergence rate of sine function nonlinear feedback is significantly slower than the other two. At the same time, Figure 15 shows that

https://doi.org/10.1017/S0373463318000024 Published online by Cambridge University Press

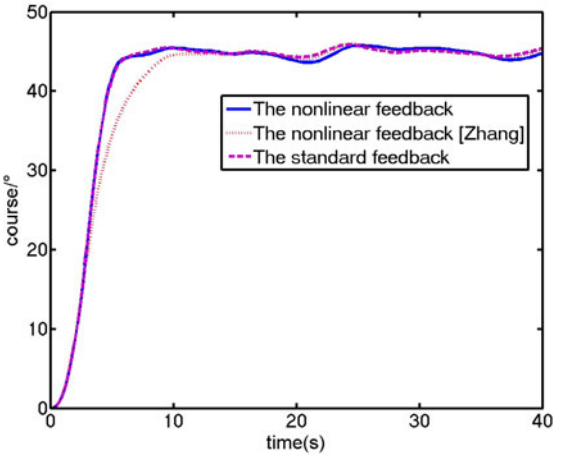


Figure 14. Course-keeping curves.

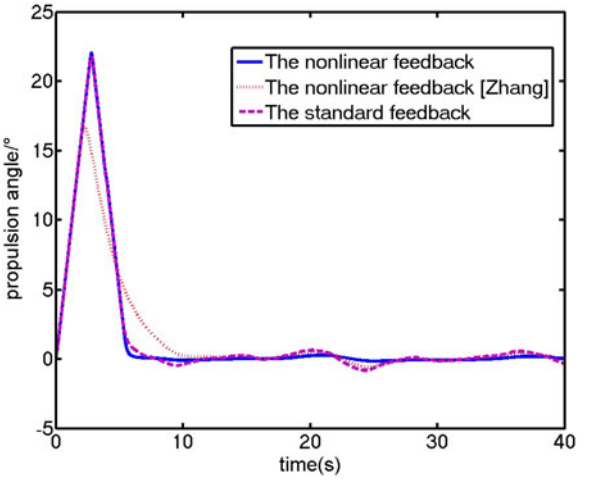


Figure 15. Propulsion angle curves.

Table 1. ITAE index.

ITAE	Value
Nonlinear feedback	251.6
Nonlinear feedback [Zhang]	372.2
Standard feedback	384.3

the propulsion angle of the nonlinear feedback proposed in this paper is more stable than the other two. It is noted that compared with sine function nonlinear feedback and standard feedback, the ITAE value of nonlinear feedback proposed in this paper drops by 32.4% and 34.5% respectively. In practical engineering, the course is allowed to fluctuate within a certain range, but the frequent fluctuation of propulsion angle is unrealistic. Therefore, compared with the other two strategies, the proposed nonlinear feedback is more suitable for practical applications.

https://doi.org/10.1017/S0373463318000024 Published online by Cambridge University Press

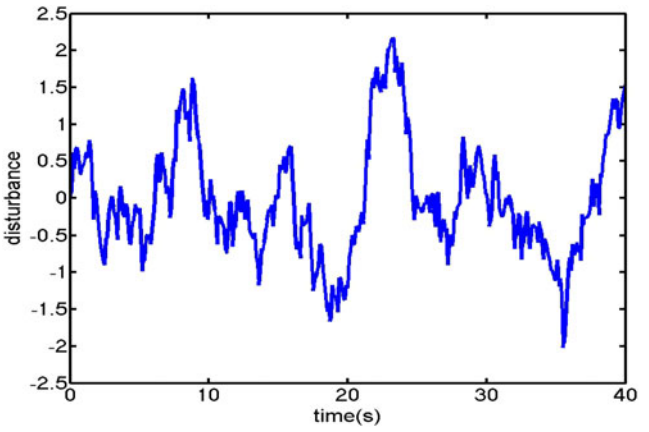


Figure 16. Strong external disturbance curve.

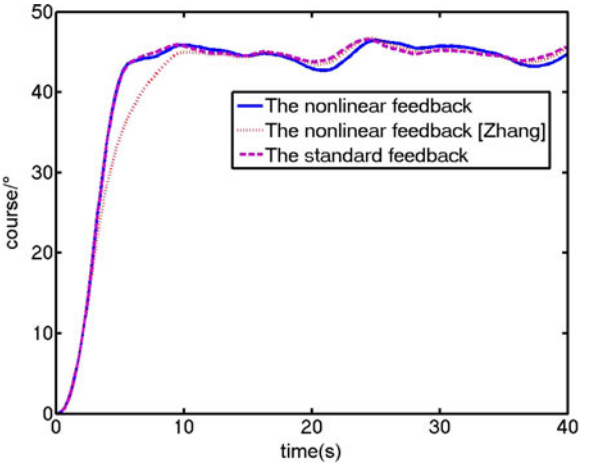


Figure 17. Course-keeping curves.

In order to verify the robustness of nonlinear feedback, the intensity of the external disturbance is increased. An enhanced external disturbance curve is shown in Figure 16, and simulation results are shown in Figures 17 and 18.

The ITAE index of propulsion angle under strong external disturbance, is shown in Table 2.

Figure 17 shows the course curves, where all three feedback strategies can keep the course near the target value. Figure 18 shows propulsion angle curves. The nonlinear feedback proposed in this paper is more stable than the other two feedback strategies. As can be seen from Table 2, the ITAE value of nonlinear feedback proposed in this paper is the smallest, decreased by 40.8% compared with standard feedback. Thus, the robustness of the proposed nonlinear feedback is proved.

https://doi.org/10.1017/S0373463318000024 Published online by Cambridge University Press

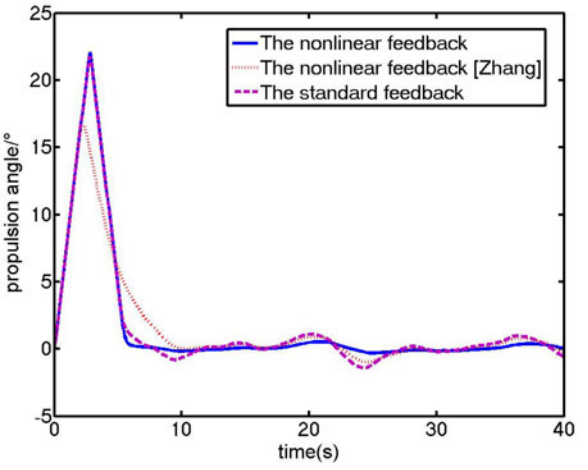


Figure 18. Propulsion angle curves.

Table 2. ITAE index (strong external disturbance).

ITAE	Value
Nonlinear feedback	316.6
Nonlinear feedback[Zhang]	481.9
Standard feedback	534.9



Figure 19. Field experiment environment.

6. ENGINEERING PRACTICE. In this Section, a set of field experiments are carried out to verify the correctness of nonlinear feedback. Field experiments are carried out in a rough sea state to better verify its robustness.

For the field experiments, the offshore wind was north-easterly, about Force 6 (Beaufort Scale), and the height of the waves were 1.25–2.5 metres. The sea conditions are illustrated in Figure 19.

https://doi.org/10.1017/S0373463318000024 Published online by Cambridge University Press

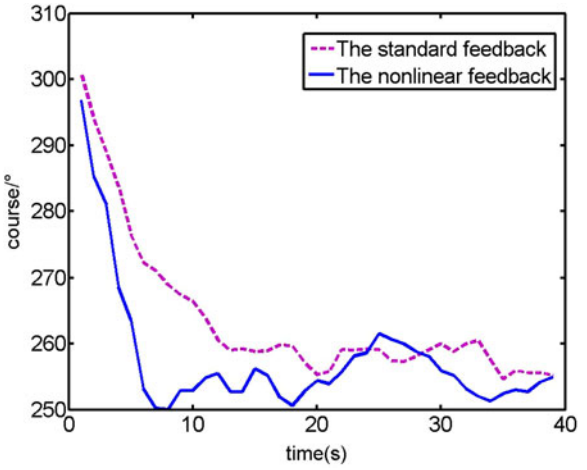


Figure 20. Course keeping curves.

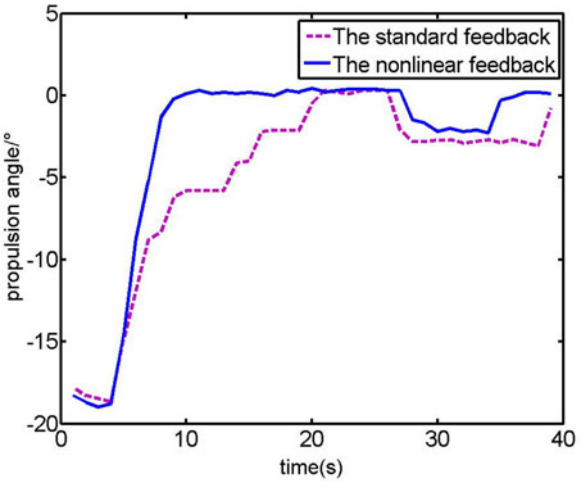


Figure 21. Propulsion angle curves.

First, we manually adjusted the initial course of the USV to about 300° and maintained its speed at about 5 m/s. After waiting for the system to be stable, the USV was adjusted to the automatic control state, and then course-keeping experiments for nonlinear feedback PD control and standard feedback PD control were carried out to authenticate each other. In order to ensure the two experiments are comparable, the initial course value of the two experiments was about 300°, and the speed of the USV was kept to about 5 m/s. Experimental results are shown in Figures 20 and 21.

Figure 20 shows a course-keeping comparison result of nonlinear feedback and standard feedback, where the initial course is about 300° and the target course is 250°. We can see clearly that unlike in the simulation, the control effect of nonlinear feedback control is better than that of standard feedback control. There are fluctuations in the control effect of nonlinear feedback control, but the standard feedback control effect finds it difficult to reach

https://doi.org/10.1017/S0373463318000024 Published online by Cambridge University Press

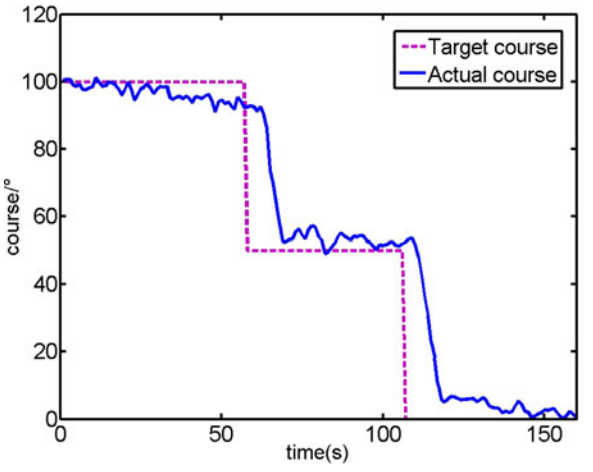


Figure 22. Course tracking curves.

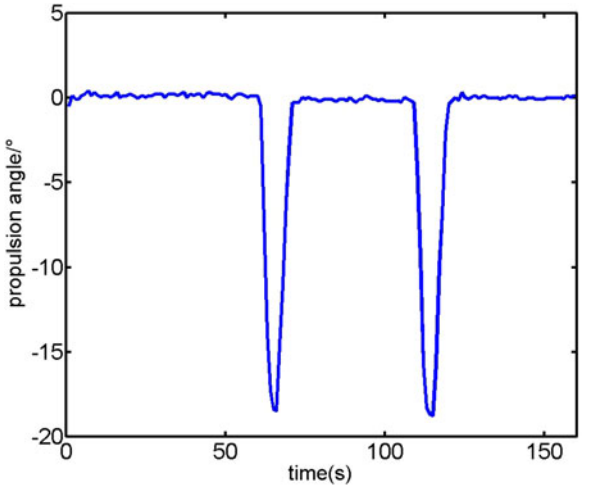


Figure 23. Propulsion angle curves.

the target course of 250°. Figure 21 shows the control outputs of the nonlinear feedback and the standard feedback. It can be clearly seen that the output of nonlinear feedback control is more stable than standard feedback control. This result can save energy and reduce friction loss.

Meanwhile, without changing any control parameters, the robustness of nonlinear feedback is verified by a course-tracking field experiment. First, the speed of the USV is kept at around 5 m/s, and we manually adjusted the initial course of the USV to about 100°. Then the USV was adjusted to the automatic control state. The first part of the field experiment was to keep the course at 100°, and then the target value of course is reduced by 50° every 55 seconds. The course tracking field experiment results are shown in Figures 22 and 23.

Figure 22 shows the nonlinear feedback control course tracking curve, and even in the case of strong external interference, the system response can track the target value well.

https://doi.org/10.1017/S0373463318000024 Published online by Cambridge University Press

As can be seen in Figure 23, in the steady state, the control output is quite stable. The correctness and superiority of the proposed nonlinear feedback are proved by a number of comparisons and a set of field experiments.

7. CONCLUSIONS. In this paper, from modelling, model identification and controller design to field experiments, a complete course-keeping scheme is proposed for a USV with pod-like propulsion. After obtaining the response model of the USV, the method of system identification is used to obtain model parameters. Then a novel nonlinear feedback strategy is presented and then applied to design a course controller for a USV. Simulation results have been presented to illustrate the correctness and effectiveness of the proposed algorithm. The proposed nonlinear feedback PD course controller is applied to a real vessel experiment, and the correctness of this paper's view is further verified. This work did not attend to every detail of the control task. For example, the control parameters cannot be adjusted automatically. This will be addressed in future work.

FINANCIAL SUPPORT

This work is partially supported by "the Nature Science Foundation of China" (grant NO. 51609033 and 51679024), "the Nature Science Foundation of Liaoning Province of China" (grant NO. 2015020022) and "the Fundamental Research Funds for the Central Universities" (grant NO. 3132014321 and 3132016315).

REFERENCES

Abkowitz, M A. (1964). Lectures on ship hydrodynamics–Steering and manoeuvrability. *Report Hy-5, Hydro-and Aerodynamic Laboratory, Denmark*.

Du, J., Guo, C. and Yang, C. (2006). Adaptive tracking controller design for ship course nonlinear system. *Journal of Applied Science*, **24**(1), 83–88.

Fan, Y., Sun, X., Wang, G. and Guo, C. (2015). On fuzzy self-adaptive PID control for USV course. *34th China Control Conference (CCC), Hangzhou China, IEEE*, 8472–8478.

Fan, Y., Ge, Z., Zhao, Y. and Wang, G. (2015) Design of information network and control system for USV. *54th IEEE Annual Conference of the Society of Instrument and Control Engineers of Japan*, 1126–1131.

Fang, M.C. and Luo, J.H. (2007). On the track keeping and roll reduction of the ship in random waves using different sliding mode controllers. *Ocean Engineering*, **34**(3/4), 479–488.

Gao, J. and Chen, G.Y. (2010). Fuzzy sliding mode control and simulation for ship's course steering. *Journal of Jiangsu University of Science and Technology: Natural Science Edition*, **24**(4), 372–376.

Jia, X. and Yang, Y. (1999). *The mathematical model of ship motion mechanism modeling and identification modeling*. Dalian Maritime University Press, 234–238.

Li, J., Li, T. and Li, Y. (2012). NN-based adaptive dynamic surface control for a class of nonlinear systems with input saturation. *7th Industrial Electronics and Applications (ICIEA), Singapore, IEEE*, 570–575.

Li, Y. and Tong, S. (2016). Adaptive neural networks decentralized FTC design for nonstrict-feedback nonlinear interconnected large-scale systems against actuator faults, *IEEE Transactions on Neural Networks and Learning Systems*, **28**(11), 2541–2554.

Li, Y., Tong, S., Liu, L. and Feng, G. (2017). Adaptive output-feedback control design with prescribed performance for switched nonlinear systems. *Automatica*, 225–231.

Li, R., Li, T. Bu, R., Zheng, Q. and Chen, P. (2013). Active Disturbance Rejection with Sliding Mode Control Based Course and Path Following for Underactuated Ships. *Mathematical Problems in Engineering*, (1), 1–9.

Mu, D., Wang, G., Fan, Y. and Zhao, Y. (2017). Modeling and Identification of Podded Propulsion Unmanned Surface Vehicle and Its Course Control Research. *Mathematical Problems in Engineering*, (2), 1–13.

Nomoto, K., Taguchi, K., Honda, K. and Hirano, S. (2009). On the Steering Qualities of Ships. *International Shipbuilding Progress*, **4**(35), 354–370.

https://doi.org/10.1017/S0373463318000024 Published online by Cambridge University Press

Norrbin, N.H. (1971). Theory and Observations on the Use of a Mathematical Model for Ship Manoeuvring in Deep and Confined Waters. *SSPA Report No.68*.

Peng, Z., Wang, D., Wang, W. and Liu, L. (2016). Neural adaptive steering of an unmanned surface vehicle with measurement noises. *Neurocomputing*, **186**(C), 228–234.

Sakuma, S. and Naruse, T. (2016). On the Steering Quality Indices of Some POD. *Driven Ships*, **23**, 27–32.

Sarda, E.I., Bertaska, I.R., Qu, A. and Ellenrieder, K.D.V. (2015). Development of a USV station-keeping controller. *Oceans, Genoa, Italy*, *IEEE*, 1–10.

Skjetne, R., Smogeli, Ø. and Fossen, T.I. (2004). Modeling, Identification, and Adaptive Maneuvering of CyberShip II: A complete design with experiments. *IFAC Proceedings Volumes*, **37**(10), 203–208.

Sonnenburg, C.R. and Woolsey, C.A. (2013). Modeling, identification, and control of an unmanned surface vehicle. *Journal of Field Robotics*, **30**(3), 371–398.

Tong, S., Huo, B. and Li, Y. (2014). Observer-Based Adaptive Decentralized Fuzzy Fault-Tolerant Control of Nonlinear Large-Scale Systems With Actuator Failures. *IEEE Transactions on Fuzzy Systems*, **22**(1), 1–15.

Wang, D. and Huang, J. (2005). Neural network-based adaptive dynamic surface control for a class of uncertain nonlinear systems in strict-feedback form. *IEEE Transactions on Neural Networks*, **16**(1), 195–202.

Yuan, L. and Wu, H.S. (2010). Terminal sliding mode fuzzy control based on multiple sliding surfaces for nonlinear ship autopilot systems. *Journal of Ship and Ocean Engineering: English Edition*, **9**(4), 425–430.

Yang, C., Jia, X. and Bi, Y. (2001). *Ship rudder roll stabilization and robust control*. Dalian Maritime University Press.

Zhang, X.K. and Jia, X.L. (2002). Simplification of H∞ mixed sensitivity algorithm and its application. *Automatic Control and Computer Sciences*, **36**(3), 28–33.

Zhang, X.K., Yang, G., Zhang, Q. and Zhang, Y. (2017). Improved Concise Backstepping Control of Course Keeping for Ships Using Nonlinear Feedback Technique. *Journal of Navigation*, **70**(6), 1401–1414.

Zhang, X. and Zhang, G. (2016). Design of Ship Course-Keeping Autopilot using a Sine Function-Based Nonlinear Feedback Technique. *Journal of Navigation*, **69**(2), 246–256.

Zhang, X. (2011). Control Algorithm for Autopilot Driven by Sine of Course Deviation. *Navigation of China*, **34**(1), 1–4.

https://doi.org/10.1017/S0373463318000024 Published online by Cambridge University Press